

Monitoring the high-energy radiation environment of exoplanets around low-mass stars with SPARCS (Star-Planet Activity Research CubeSat)

Paul A. Scowen^{*a}, Evgenya L. Shkolnik^a, David Ardila^b, Travis Barman^c, Matthew Beasley^d, Judd Bowman^a, Michael Fitzgerald^a, Varoujan Gorjian^b, Daniel C. Jacobs^a, April Jewell^b, Joe Llama^e, Victoria Meadows^f, Shouleh Nikzad^b, Constance Spittler^a, Mark Swain^b, Robert Zellem^b

^aSchool of Earth and Space Exploration, Arizona State University, 781 E. Terrace Mall, Tempe, AZ, USA 85287-6004; ^bJet Propulsion Laboratory, 4800 Oak Grove Dr, Pasadena, CA 91109; ^cLunar and Planetary Lab, University of Arizona, 1415 N 6th Ave, Tucson, AZ 85705; ^dSouthwest Research Inc., 1050 Walnut St #300, Boulder, CO 80302; ^eLowell Observatory, 1400 W Mars Hill Rd, Flagstaff, AZ 86001; ^fDept. of Astronomy, University of Washington, 3910 15th Ave NE, Seattle WA 98195-0002

ABSTRACT

Roughly 40 billion M dwarfs in our galaxy host at least one small planet in the habitable zone (HZ). The stellar ultraviolet (UV) radiation from M dwarfs is strong and highly variable, and impacts planetary atmospheric loss, composition and habitability. These effects are amplified by the extreme proximity of their HZs (0.1–0.4 AU). Knowing the UV environments of M dwarf planets will be crucial to understanding their atmospheric composition and a key parameter in discriminating between biological and abiotic sources for observed biosignatures. The Star-Planet Activity Research CubeSat (SPARCS) will be a 6U CubeSat devoted to photometric monitoring of M stars in the far-UV and near-UV, measuring the time-dependent spectral slope, intensity and evolution of low-mass star high-energy radiation.

Keywords: Cubesat, Ultraviolet, Imaging, Photometry, Low Mass Stars, Exoplanet, Habitability, Radiation Environment

1. INTRODUCTION

There are roughly 40 billion habitable zone (HZ) terrestrial planets orbiting low mass stars, also known as M dwarfs (0.1–0.6 M_{\odot}) in our galaxy alone [1,2]. The stellar ultraviolet (UV) radiation from M dwarfs is strong and highly variable, and impacts planetary atmospheric loss, composition and habitability. These effects are amplified by the extreme proximity of their HZs (0.1–0.4 AU; [3]). Unlike solar-type stars, M dwarfs are known to stay active with high emission levels and frequent flares throughout their lives ([6]; Sec. 1.2.2). The effects of sustained high levels of stellar activity on planetary atmospheres have not been studied since UV flare rates and energies across timescales longer than a few hours are not known.

Knowing the UV environments of M dwarf planets will be crucial to understanding their atmospheric composition and a key parameter in discriminating between biological and abiotic sources for observed biosignatures (see Figure 1). The UV flux emitted during the super-luminous pre-main sequence phase of M stars drives water loss and photochemical O_2 buildup for terrestrial planets within the HZ [5]. This phase can persist for up to a billion years for the lowest mass M stars (e.g., [6,7]). Afterwards, UV-driven photochemistry during the main sequence phase strongly affects a planet's atmosphere (e.g., [8]; Figure 1), could limit the planet's potential for habitability, and may confuse studies of habitability by creating false chemical biosignatures. It is necessary to determine the lifetime exposure of such planets to stellar UV radiation, from quiescent and flare emission levels, and explore the limitations on the evolution of life and our potential to identify it. The upcoming James Webb Space Telescope (JWST) will characterize HZ M dwarf planets and attempt the first spectroscopic search for life beyond the Solar System.

*paul.scowen@asu.edu; phone 1 480 965-0938; fax 1 480 965-8102; sese.asu.edu

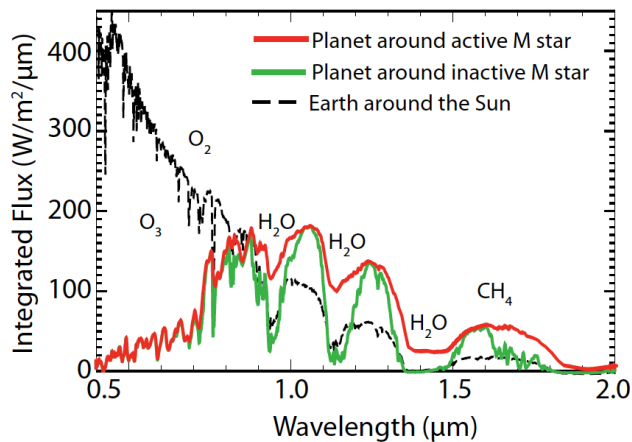


Figure 1. The stellar UV flux has a dramatic effect on a planet’s atmospheric content. The plot shows an Earth-like planet spectrum in the habitable zone of an active (red) and inactive (green) M4 dwarf. The spectrum of the Earth around the Sun is shown black for comparison. (Adapted from [4])

Observed Galaxy Evolution Explorer (GALEX) FUV and NUV median fluxes drop as stars age [6], but yet the range of UV emission levels from M stars still spans 1 to 2 orders of magnitude at every age. These large flux excursions from the median are likely caused by frequent flaring events and large differences in intrinsic flux levels between stars. Miles and Shkolnik [10] analyzed the GALEX NUV and FUV fluxes of hundreds of old M dwarfs with two or more observations of each star recorded randomly over the nine-year mission. They show that an old M0 dwarf typically varies in the NUV by a few percent while an M5 varies by about 35%. In the FUV, there is consistent median variability at 25%, yet a wide range exists at each spectral type (Figure 2).

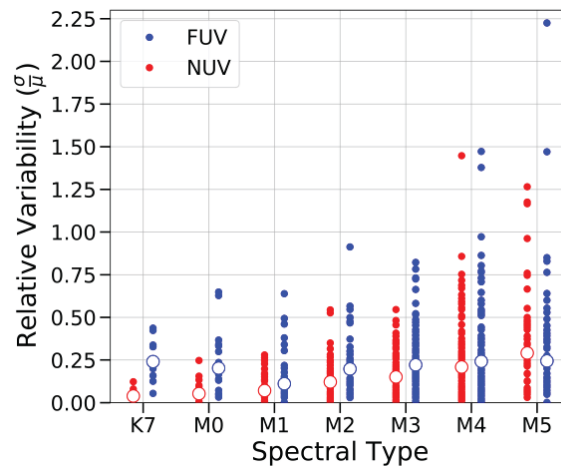


Figure 2. SPARCS’ required photometric precision is set by the FUV and NUV variability at each spectral type. We plot the average variation (σ/μ) for M dwarfs observed more than once with GALEX. Medians are shown as larger circles [10].

A UV characterization survey of M dwarfs, the most common of planet hosts, is an ideally matched experiment for a CubeSat mission. Reasons include that UV astronomy cannot be done from the ground because of Earth’s atmospheric absorption, that photometry of nearby sources is an efficient use of a small aperture, and that unlike the Hubble Space Telescope (HST) whose time is shared annually by hundreds of programs, a CubeSat can provide dedicated space-based long-term monitoring in the UV.

The NASA-funded Star-Planet Activity Research CubeSat (SPARCS) observatory (Figure 3) will be the first mission to provide the time-dependent spectral slope, intensity and evolution of M star UV radiation. SPARCS will be a 6U CubeSat devoted to monitoring ≈ 20 M stars in two UV bands: SPARCS far-UV (S-FUV: 153–171 nm) and SPARCS near-UV (S-

NUV: 260–300 nm). SPARCS bands include emission lines formed at various stellar heights to measure variability and guide new upper-atmospheric stellar models, with which we aim to predict the extreme-UV (EUV; 10–90 nm) radiation (Figure 4, left).

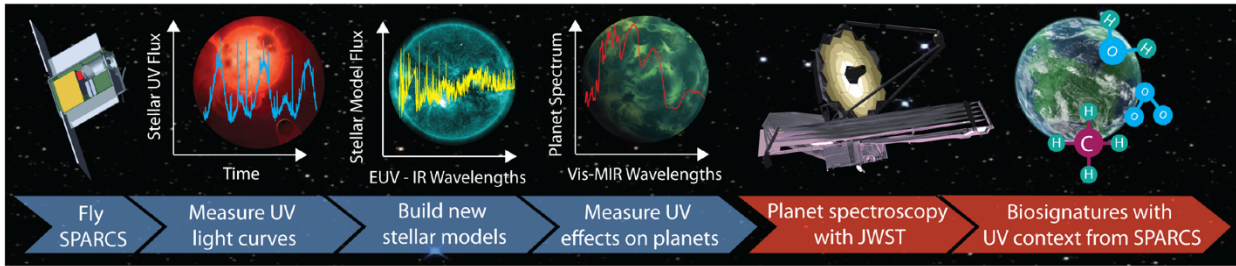


Figure 3. The SPARCS mission science goals. After launch and commissioning, the telescope will monitor the rotational and flare variability in the FUV and NUV of M stars, from young to old. Those data will be used to guide new upper-atmosphere models, which will be used to predict the entire spectral range including the EUV. These empirically-motivated models will provide accurate inputs to the exoplanetary photochemistry models needed to best interpret planetary spectra observed by upcoming missions such as JWST.

The UV emission probed by SPARCS can photodissociate important diagnostic molecules in a planetary atmosphere, such as water (H₂O), ozone (O₃), sulfur dioxide (SO₂), a signature of volcanic activity, and ammonia (NH₃), an important source of the nitrogen required to build amino acids (Figure 4, right).

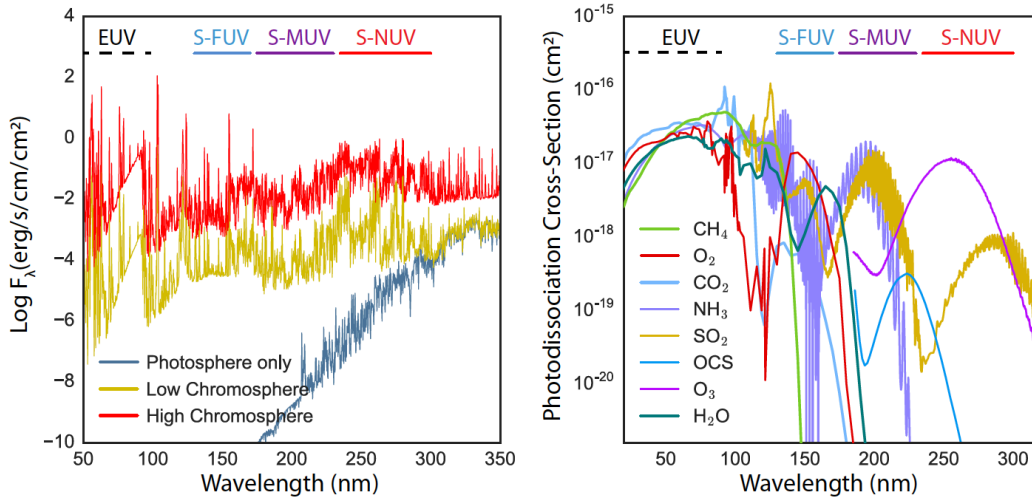


Figure 4. SPARCS UV filters probe key spectral regions important for both M dwarf non-thermal emission and exoplanet atmospheric molecules. Left: Comparison of M dwarf model atmospheres. UV emission in M dwarfs is dominated by the upper-atmosphere activity, which is traced by SPARCS bands [9]. SPARCS baseline (S-FUV and S-NUV) and threshold (S-MUV) filter ranges are shown. Right: SPARCS measurements constrain the unobservable EUV fluxes, which control the photodissociation of many common planetary atmospheric trace gases, including biosignatures.

The S-FUV filter transmission peaks between the C IV doublet (155 nm), formed in the transition region at $\sim 10^5$ K, and the He II line (164 nm), formed in the corona at $\sim 10^7$ K. The strongest feature in the S-NUV bandpass is the upper-chromospheric Mg II doublet (280 nm) formed at $\sim 10^4$ K, similar to, and correlates with, Lyman- α (121.5 nm; [11]). A threshold S-MUV filter has been defined in the case that the S-FUV filter proves difficult to manufacture. For each target, SPARCS will observe nearly continuously between one and three complete stellar rotations (4–45 days) over a mission lifetime of 2 years.

For all types of exoplanets, from Earths to Jupiters, photochemical atmosphere models require realistic input stellar fluxes across the UV range [8,12-16]. As standard stellar atmosphere models [17,18] substantially under-predict UV emission

from M dwarfs (Figure 3, left), SPARCS UV bands will also allow for the prediction of the observationally inaccessible EUV radiation, which photoionizes, heats and inflates a planet’s upper-atmosphere promoting atmospheric erosion [19]. EUV photons also generate hazes [20,21], which strongly affect the observed planet spectrum. Observations of featureless planet spectra (e.g., [22,23]) show that hazes in planets around M dwarfs might in fact be quite common, probably generated by the star’s UV flux.

2. MISSION SCIENCE GOALS

2.1 Stellar Variability: UV Amplitude and Frequency Distribution

While GALEX FUV and NUV fluxes drop as stars age [6], the range of UV emission levels from M dwarfs still spans 1–2 orders of magnitude at every age. These large flux excursions are likely caused by frequent flaring events and intrinsic emission variations from star to star. SPARCS aim to measure these difference and the flare frequency distributions for each star with cadences and baselines not yet probed in the UV.

What flare rate might we expect? Using round-the-clock visible-light monitoring, Davenport et al. [24] analyzed 11 months of Kepler data of the active M4 star GJ 1243 and found over 6000 individual flaring events averaging 19 flares/day. For SPARCS this would mean a flare nearly every orbit. Even for the slow-rotator Proxima Centauri, Davenport et al. [25] report a strong optical light flare rate of >2/day, with weaker flares predicted to occur 63 times per day. As shown in Figure 5, weak optical flares will be very strong in the UV, particularly in the S-FUV band.

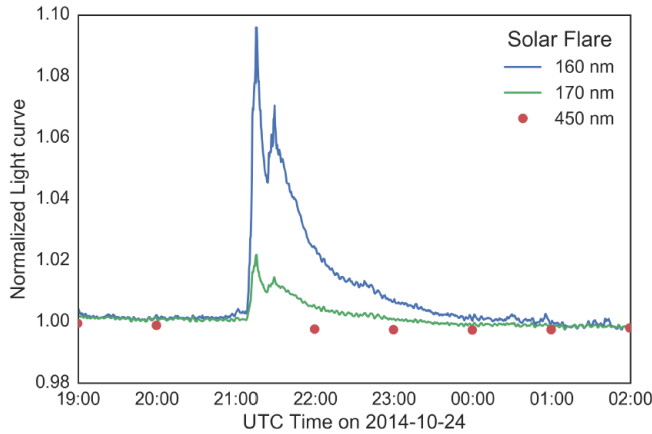


Figure 5. The S-FUV bandpass is extremely sensitive to flare activity. This disk-integrated solar flare was observed by the Atmospheric Imaging Assembly onboard NASA’s Solar Dynamics Observatory, and shows that activity appearing weak (or undetected) in the optical will be strong in the UV (Llama et al., in prep.).

2.2 SPARCS Targets: Mapping the UV Evolution of Planetary Systems

SPARCS targets include: young stars currently forming terrestrial planets (e.g., 10 Myr-old AU Mic; [26]), UV bright stars known to be active (e.g., AD Leo; [27]), intermediate age M stars (e.g., 300 Myr old DS Leo; [28]), and old, relatively-inactive, M dwarfs including known planet hosts with transiting planets. GALEX data were used to estimate exposure times and characterize each field of view (FOV) in the UV (Section 5). As new exoplanet discoveries are made by TESS and ground-based surveys, we can add them to the target list.

2.3 Building Synthetic EUV–NUV M Dwarf Upper-Atmosphere Spectra and Applications to Planet Atmosphere Photochemical Models

Standard stellar atmosphere models [17,18] substantially under-predict UV emission from M dwarfs (Figure 4, left). These models are intended primarily for comparisons with optical/infrared observations, they lack any prescription for the lowest density regions of the upper-atmosphere (i.e., the chromosphere, transition region, and corona), and assume local thermodynamic equilibrium (LTE). It is, therefore, not surprising that standard M dwarf model grids do not compare well to the observed UV fluxes (e.g., [29]). If models are to be used to predict the EUV to NUV fluxes from M dwarfs, they must be modified to include upper-atmosphere emission measures and non-LTE radiative transfer.

We will use the unique time-domain nature of SPARCS observations to construct a new M dwarf model atmosphere grid, during quiescent and flare states of young and old M stars, suitable for predicting the evolution and variability of the EUV-to-NUV flux. The models are being developed using the non-LTE atmosphere code PHOENIX [30,31,32], which includes an up-to-date set of atomic-level data suitable for the high temperatures and low densities found in M dwarf upper-atmospheres [33]. We are following the work of [34,35 and 36] and will superimpose ad hoc thermal models for the upper-atmosphere onto a new “photosphere only” M dwarf grid calculated using PHOENIX. Figure 4 (left) illustrates an example of new upper-atmosphere models and the level of EUV fluxes one might expect for M dwarf planet hosts.

These empirically-guided stellar models will provide the exoplanetary community with the much-needed input spectra for time-dependent photochemical, climate and atmospheric escape models for terrestrial exoplanets. In turn, these planet atmosphere models will inform observations to be performed with JWST and future missions, and allow for accurate interpretation of exoplanetary spectra.

3. MISSION REQUIREMENTS

The SPARCS mission objectives are to characterize variation in M dwarfs on timescales from minutes up to the known stellar rotation period. The types of variation targeted range from the slow rotational modulation to prompt, intense flaring seen in both active and inactive stars. The goal is to observe enough stars to inform models across a range of stellar ages and masses.

The top-level requirements are for a sensitivity level suitable to detect quiescent NUV emission of 22 stars, stare length and observing duty cycle to minimize interruptions to enable detection of flares. These requirements can be met by a payload comprising a 9-cm aperture telescope and two delta-doped UV sensitive CCD operating in a Sun-synchronous orbit with a 6 pm ascending node, which will provide a nearly continuous view of sources lying in the ecliptic.

The nominal mission duration is two years but a threshold period of three months will provide a significant and useful data set in its own right as well as good initial demonstration of the science capability. The nominal spectral requirement is simultaneous observation in the S-FUV and S-NUV, which respectively probe the transition region and chromosphere of the star. This requirement can be met by a two-channel UV camera with the beam split by a dichroic; both channels include filters optimized for the band of interest. The FUV channel requires a custom filter made using a novel technique which has been used in different contexts, for this reason a threshold option is to replace FUV with a longer wavelength that probes the spectral index of the continuum emission. Accuracy suitable for measuring variation at a level of 3/MAD (mean absolute deviation based on results of [10]) is set by a requirement for 10% accuracy on absolute flux relative to known standards.

4. MISSION DESIGN

While still in formulation, the mission has already completed its Systems Requirements Review and is advancing to the design of the payload and spacecraft. Figure 6 shows the current working solid model for the spacecraft. SPARCS will occupy a 6U form factor and have fold-out solar panels and thermal radiators. The telescope (see Section 5.1) will occupy 1.5U and be positioned on the right-hand side of the volume. Behind the telescope will be the SPARCS camera (SPARCam) detectors and readout electronics (see Section 5.3). The left-hand side of the spacecraft will contain the rest of the subsystems for the operation of the mission (Attitude Control System (ACS), Power, Communications, Command & Data Handling, etc.).

As part of the mission design we have conceived of a concept of operations that enables observations of the 22 targets over the mission lifetime while providing for adequate power, communications links, and thermal control to meet and maintain the operational requirements of the mission. The architecture that has flown from that statement of operations is shown in Figure 7. We plan to work and share operations and responsibilities with our spacecraft vendor partner (yet to be determined) for command and control through the Mission Operations Center (MOC) as well as development of the spacecraft during I&T. The majority of data processing and initial archiving will be conducted at Arizona State University with communications enabled through a network of ground-based stations. Final data products will be archived at the Mikulski Archive for Space Telescopes (MAST).

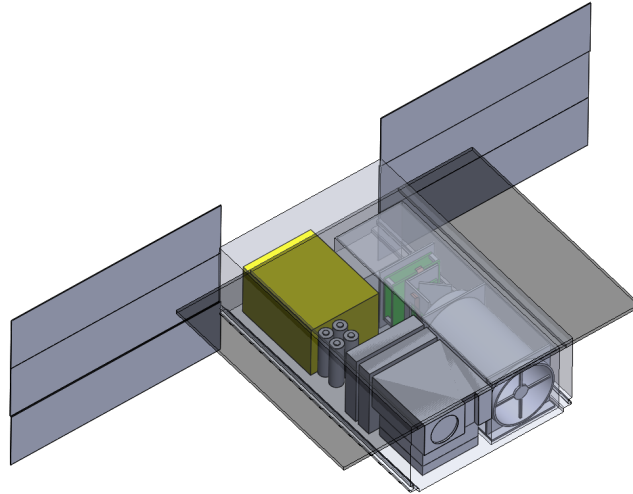


Figure 6. Notional solid model of the SPARCS spacecraft including the different subsystems in the mission design.

The functional block diagram for the spacecraft itself is detailed in Figure 8. Each subsystem has requirements that it must meet and notional elements of those subsystems are indicated. Note the functional elements that comprise the ACS system that feeds into the Guidance Navigation and Control (GN&C) subsystem. Where appropriate the interfaces between the subsystems have been indicated along with type. It should be emphasized that we are in the earliest of stages with the mission design so it is likely that details will change before we complete Critical Design Review.

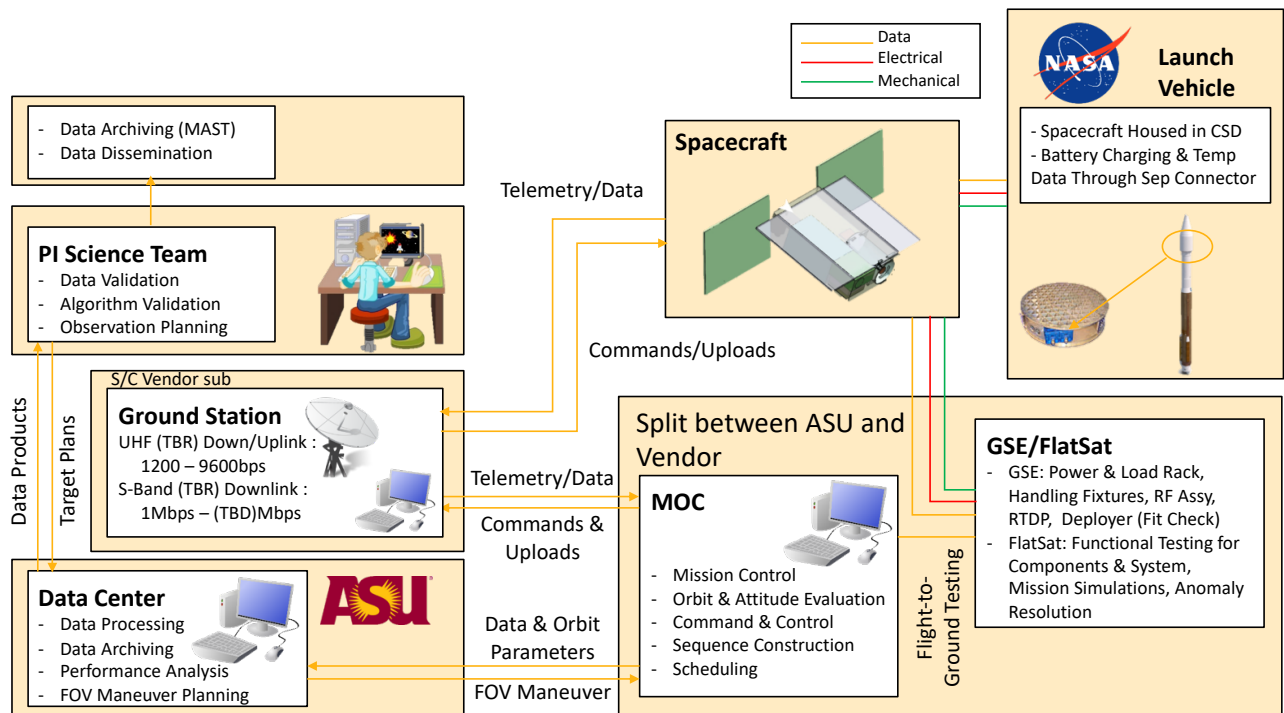


Figure 7. The mission architecture. The functional elements of the mission system, based in part on our current concept of operations, are detailed with their interdependencies and responsibilities for member institutions.

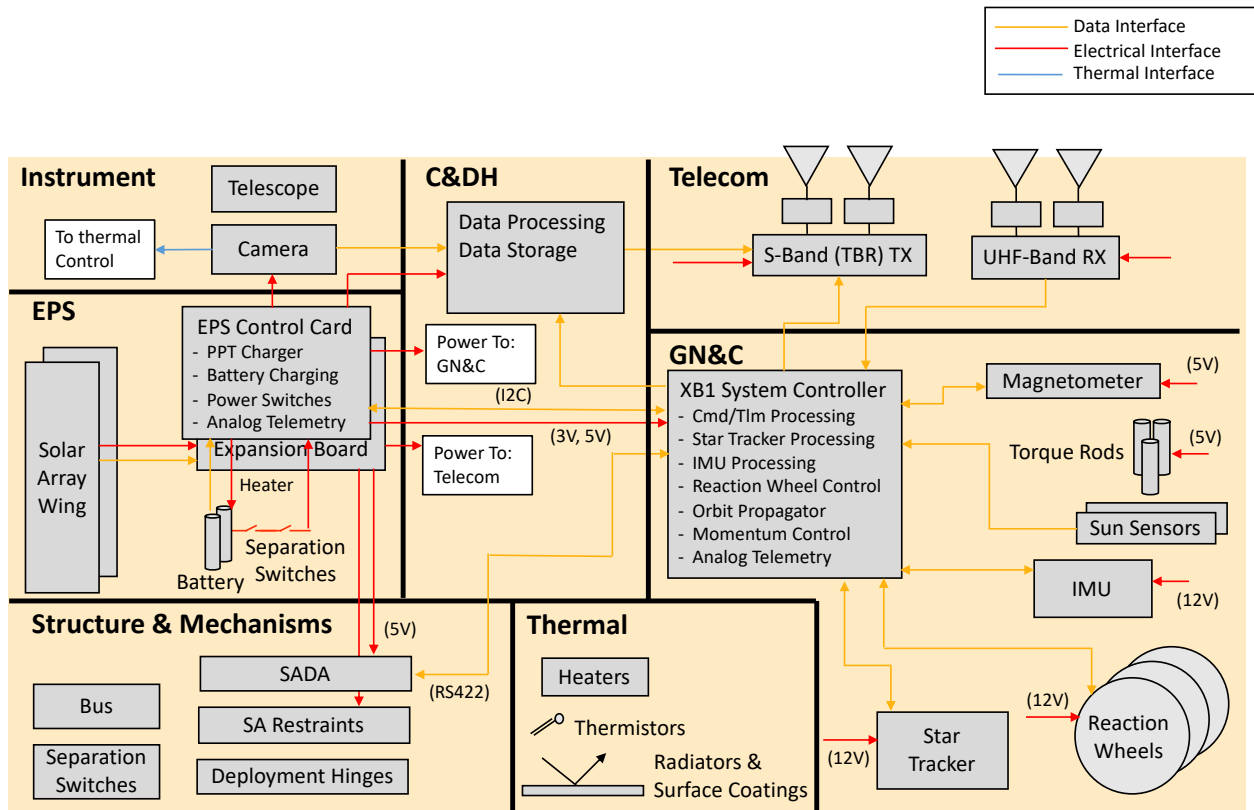


Figure 8. SPARCS spacecraft block diagram. The functional subsystems for the mission design are shown with notional constituent elements and expected interfaces between those subsystems.

5. MISSION PAYLOAD

5.1 The SPARCS Telescope

We have baselined a Ritchey–Chrétien (R-C) telescope which is a specialized variant of the Cassegrain telescope that utilizes hyperbolic primary and secondary mirrors. The fundamental advantage of this design is that it enhances off-axis optical performance by reducing Coma, a common aberration of Cassegrain telescopes.

The R-C design is a well-developed design that allows for excellent performance over larger field angles. This telescope design has an impressive heritage for both ground applications (Subaru telescope at Mauna Kea Observatory, Keck observatory) as well as space telescopes (Hubble Space Telescope, Spitzer Space Telescope). The absence of refractive elements makes the design completely achromatic, promotes higher throughput and allows for the assembly, alignment and test of the system to be performed using visible light sources and detectors, thus significantly reducing assembly and test complexity and cost.

Ultra-low expansion glass has been baselined for the optical elements. Such materials provide excellent thermal stability, and are capable of being figured and polished to meet the system requirements. The peak-to-valley wavefront requirement for the mirrors is 1/8 wave at 632 nm. The surface micro-roughness is specified at less than 10 Angstroms, which will prevent unwanted scatter of the incoming UV radiation. As the mechanical design matures, stray light will be controlled using light baffles which will prevent unwanted radiation from reaching the detector.

For the candidate mirror we have baselined the Hubble coating prescription to achieve the required reflectivity and will subcontract with NASA Goddard Space Flight Center (GSFC) to have this coating applied to the optics after manufacture.

Opto-mechanical Construction

The SPARCS telescope assembly (see Figure 9) will be built in an athermal manner in order to maintain focus and boresight throughout the required temperature range of -40 to 60C. The design incorporates invar mating pieces that

adhere to the 10:1 aspect ratio Zerodur Primary and Secondary optics. The metering tube will be constructed of High Modulus Carbon fiber reinforced polymer (CFRP) composite, to allow for a stiff structure and greatly reduce overall mass. Due to the anisotropic nature of CFRP, the layup of the metering tube shall be tailored in certain percentages of unidirectional, forty-five degree, and zero degree oriented layers in order to achieve an axial CTE of zero ppm/degree Celsius. As a result, the radial coefficient of thermal expansion (CTE) of the metering tube will be 20 ppm/°C. In order to account for the radial CTE, Ti6Al-4V parts will be used for the spider and Primary mirror rear structure with an athermally designed bond to the CFRP tube. Per the NASA GSC-15506-1 design guideline for bonding composites to metals, the telescope metering tube will incorporate the tape-setback method to maximize the strength and reliability of the bond joint. Finally, the invar optical mounts will bolt via flexure pads to the titanium structure components.

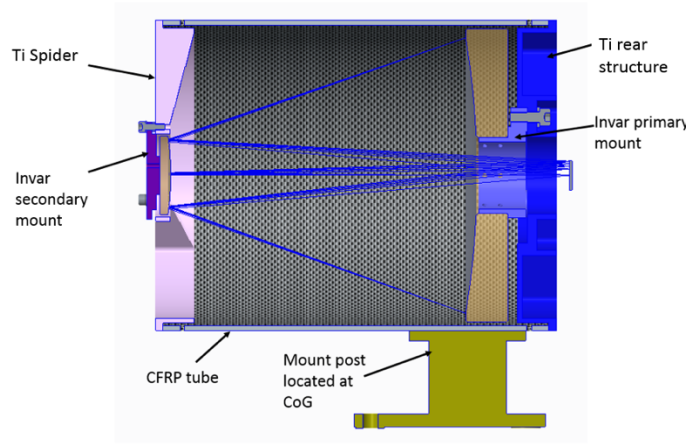


Figure 9. Overall layout of SPARCS telescope

5.2 Use of a Dichroic in the Optical Design

At the earliest of stages in the SPARCS mission, it became apparent that significant scientific gain can be achieved through simultaneous observation of FUV and NUV channels for a given target. The original proposal used a concept of operations that would “nod” the spacecraft back and forth between the separate FUV and NUV fields of view (read: detectors) but this meant that any given observation would miss the co-temporal evolution of emission from the other passband. It was proposed that the introduction of a dichroic in the optical beam immediately before the detectors could enable co-temporal observations in the 2 channels at the expense of some throughput, but that this would increase the efficiency of the monitoring mission.

When considering the use of a dichroic it is useful, in this case vital, to consider what has been done before, in heritage. The photometric passbands adopted for SPARCS (see Figure 10), were motivated by those used for GALEX but with some differences to target specific atomic species in the stellar atmospheres.

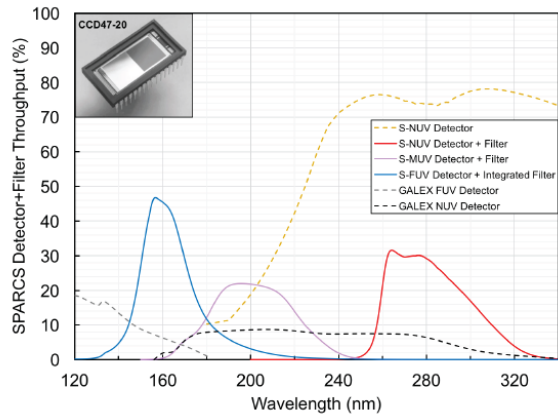


Figure 10. SPARCS passbands shown relative to the GALEX passbands

GALEX used a dichroic to achieve simultaneous observations in multiple bands. The GALEX dichroic, manufactured by Cascade Optical, had a crossover wavelength at ~ 160 nm. The SPARCS passbands differed enough from those of GALEX; so while we can use a similar approach, the SPARCS dichroic requires a crossover wavelength at $233\text{nm} \pm 5\text{nm}$.

In conceiving of using such a dichroic we had envisioned the placement to be that portrayed in Figure 12 – after the telescope but before the detectors; this would allow us to fabricate the support structure and mount the focal planes accordingly during integration & testing (I&T) at ASU.

The current state of the development involves a working model for the necessary dichroic from two companies. The performance of the two models, for reflection shortward of the crossover wavelength, and transmission longward of that crossover, is illustrated in Figure 11. While there is structure in the transmission and reflectance curves (from the multi-layer design of the optical element), the impact of this structure on the medium bands we are using for S-FUV and S-NUV is minimal when it comes to the photometric model we are carrying for the operation of the mission. The current plan is to acquire optical elements from both vendors and test them versus these model predictions and then choose the best piece for the flight design.

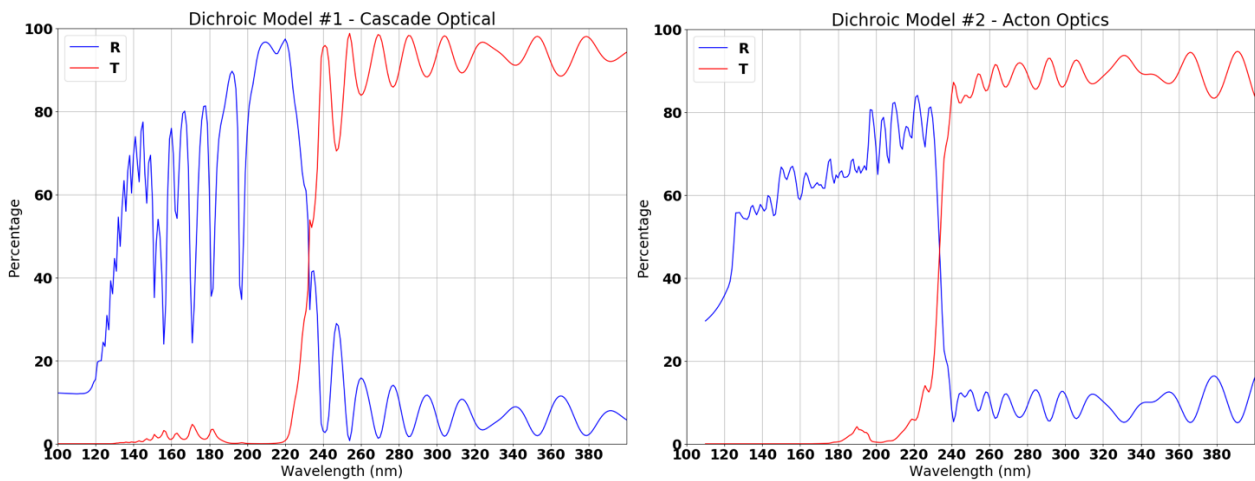


Figure 11. Current best vendor models for the SPARCS dichroic element, by permission. R is the reflection of the optic element; T is the transmission of the optic element. Left panel: model dichroic from Cascade Optical (<http://www.c-optical.com>); Right panel: model dichroic from Acton Optics (<https://www.actonoptics.com>).

5.3 The SPARCS Camera

The SPARCS camera (SPARCam) has baselined a two-channel UV camera to accommodate the two-band observation strategy for SPARCS. SPARCam’s readout electronics are based on the Jet Propulsion Laboratory’s (JPL) previous compact camera deliveries modified to function with two detectors oriented perpendicular to one another to accommodate SPARCS’ dichroic design (Figure 12).

SPARCam would advance delta-doped detectors and detector-integrated out-of-band-rejection filter technologies developed at JPL. The baseline NUV detector is a delta-doped, $1\text{k} \times 1\text{k}$ ($1\text{k} \times 2\text{k}$, frame transfer), $13\ \mu\text{m}$ CCD47-20 (Teledyne-e2v); a custom antireflection coating allows for quantum efficiency (QE) $> 70\%$ throughout the SPARCS NUV band [37]. Red-leak suppression in the NUV bandpass would be achieved with a commercial red-blocking filter that provides at least three orders of magnitude out-of-band suppression. The baseline S-FUV is also a delta-doped CCD47-20; it is optimized for the S-FUV band with a detector-integrated metal-dielectric filter designed to maximize in-band throughput while offering high out-of-band suppression [37,38]. As designed, the SPARCam FUV detector achieves peak QE $> 35\%$ in the S-FUV band and at least two orders of magnitude out-of-band suppression. An in-depth discussion of the SPARCam detectors is the subject of an accompanying proceedings manuscript [39].

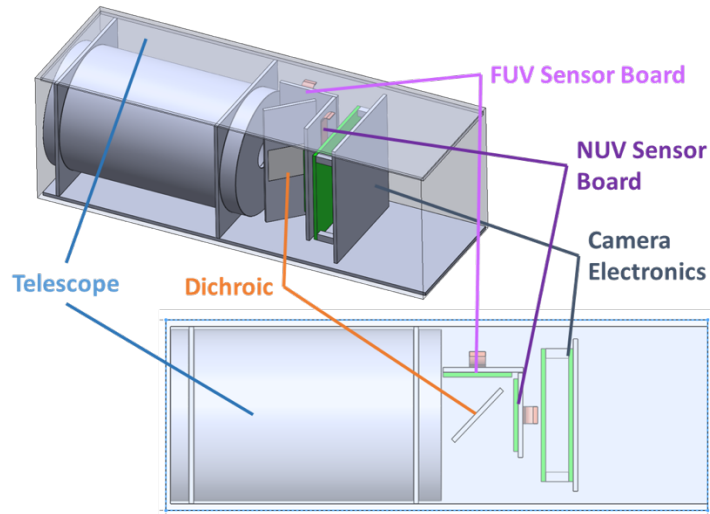


Figure 12. Notional payload configuration shows the two channel design with FUV and NUV detectors mounted perpendicular to one another to accommodate simultaneous observation in the two bands.

6. MISSION SCHEDULE AND NEXT STEPS

The SPARCS team has taken the standard NASA approach to mission planning and scheduling, having tailored traditional practices to meet the needs and scope of a CubeSat mission. Upon completion of the mission System Requirements Review (SRR) in early April, 2018, the SPARCS team received valuable feedback from an independent review board, the Astrophysics Research and Analysis (APRA) Program Scientist out of NASA HQ, and the NASA appointed Mission Manager from Wallops Space Flight Facility.

Programmatically, the SPARCS team is iteratively working to reduce schedule risk on the project in order to provide sufficient margin for design, development, and testing of the flight systems. In doing so, the project has initiated SPARCam development and major telescope procurements earlier than planned. Additionally, the project will compress schedule by conducting a standalone Preliminary Design Review (PDR) for the SPARCS payload, and a joint mission-level PDR/CDR (Critical Design Review) to allow for the design of the science payload to mature prior to implementation with the spacecraft systems. Furthermore, the project will combine the mission Pre-Ship Review and Flight Readiness Review (PSR/FRR) leading up to delivery of the SPARCS spacecraft to the designated launch provider.

Over the next 12-18 months, the SPARCS team will finalize the design of the SPARCam payload, initiate long lead flight procurements, finalize payload I&T procedures, develop a mature contamination control plan to protect critical flight UV filters, and prepare for instrument environmental testing and calibration. Development of the spacecraft will continue in parallel with the instrument schedule culminating with Spacecraft I&T notionally planned to begin in early 2021. Upon successful completion of I&T, SPARCS will be delivered for an anticipated launch in the Fall of 2021.

REFERENCES

- [1] Bochanski, John J.; Hawley, Suzanne L.; Covey, Kevin R.; West, Andrew A.; Reid, I. Neill; Golimowski, David A.; Ivezić, Željko, 2010, “The Luminosity and Mass Functions of Low-mass Stars in the Galactic Disk. II. The Field”, *AJ*, 139, 2679
- [2] Dressing, C. D., and D. Charbonneau 2015. “The Occurrence of Potentially Habitable Planets Orbiting M Dwarfs Estimated from the Full Kepler Dataset and an Empirical Measurement of the Detection Sensitivity”, ArXiv e-prints.
- [3] Kopparapu, R. K. 2013. “A Revised Estimate of the Occurrence Rate of Terrestrial Planets in the Habitable Zones around Kepler M-dwarfs”, *ApJ* 767, L8, 5 pp.
- [4] Rugheimer, S., L. Kaltenegger, A. Segura, J. Linsky, and S. Mohanty 2015. “Effect of UV Radiation on the Spectral Fingerprints of Earth-like Planets Orbiting M Stars”, *ApJ* 809, 57
- [5] Luger, R., and R. Barnes 2015. “Extreme Water Loss and Abiotic O₂ Buildup on Planets Throughout the Habitable Zones of M Dwarfs”, *Astrobiology* 15, 119–143
- [6] Shkolnik, E. L., and T. S. Barman 2014. “HAZMAT. I. The Evolution of Far-UV and Near-UV Emission from Early M Stars”, *AJ* 148, 64, 14pp.
- [7] Schneider, Adam C.; and Shkolnik, Evgenya L., 2018, “HAZMAT. III. The UV Evolution of Mid- to Late-M Stars with GALEX”, *AJ*, 155, 122
- [8] Segura, A., L. M. Walkowicz, V. Meadows, J. Kasting, and S. Hawley 2010. “The Effect of a Strong Stellar Flare on the Atmospheric Chemistry of an Earth-like Planet Orbiting an M Dwarf”, *Astrobiology* 10, 751–771
- [9] Peacock, S., T. Barman, and E. Shkolnik 2015. “Understanding the Early Evolution of M dwarf Extreme Ultraviolet Radiation”, In AAS/Division for Planetary Sciences Meeting Abstracts, Volume 47 of AAS/Division for Planetary Sciences Meeting Abstracts, pp. 404.06.
- [10] Miles, B., and E. L. Shkolnik 2017. “HAZMAT II: Ultraviolet Variability of Low-Mass Stars in the GALEX Archive”, *AJ*
- [11] Linsky, J. L., K. France, and T. Ayres 2013. “Computing Intrinsic LY ϵ Fluxes of F5 V to M5 V Stars”, *ApJ* 766, 69, 10 pp.
- [12] Line, M. R., M. C. Liang, and Y. L. Yung 2010. “High-temperature Photochemistry in the Atmosphere of HD 189733b”, *ApJ* 717, 496–502.
- [13] Kaltenegger, L., A. Segura, and S. Mohanty 2011. “Model Spectra of the First Potentially Habitable Super-Earth G1581d”, *ApJ* 733, 35, 12 pp.
- [14] Hu, R., S. Seager, and W. Bains 2012. “Photochemistry in Terrestrial Exoplanet Atmospheres. I. Photochemistry Model and Benchmark Cases”, *ApJ* 761, 166, 29 pp.
- [15] Kopparapu, R. K., J. F. Kasting, and K. J. Zahnle 2012. “A Photochemical Model for the Carbon-rich Planet WASP-12b”, *ApJ* 745, 77, 10 pp.
- [16] Moses, J. I., M. R. Line, C. Visscher, M. R. Richardson, N. Nettelmann, J. J. Fortney, T. S. Barman, K. B. Stevenson, and N. Madhusudhan 2013. “Compositional Diversity in the Atmospheres of Hot Neptunes, with Application to GJ 436b”, *ApJ* 777, 34, 23 pp.
- [17] Hauschildt, P. H., E. Baron, and F. Allard 1997. “Parallel Implementation of the PHOENIX Generalized Stellar Atmosphere Program”, *ApJ* 483, 390–398.
- [18] Allard, F., P. H. Hauschildt, D. R. Alexander, A. Tamanai, and A. Schweitzer 2001. “The Limiting Effects of Dust in Brown Dwarf Model Atmospheres. *ApJ* 556, 357–372
- [19] Koskinen, T. T., R. V. Yelle, P. Lavvas, and N. K. Lewis 2010. “Characterizing the Thermosphere of HD209458b with UV Transit Observations”, *ApJ* 723, 116–128
- [20] Arney, G., S. D. Domagal-Goldman, V. S. Meadows, E. T. Wolf, E. Schwieterman, B. Charnay, M. Claire, E. H’ebard, and M. G. Trainer 2016. “The Pale Orange Dot: The Spectrum and Habitability of Hazy Archean Earth”, *Astrobiology* 16, 873–899
- [21] Segura, A., J. F. Kasting, V. Meadows, M. Cohen, J. Scalo, D. Crisp, R. A. H. Butler, and G. Tinetti 2005. “Biosignatures from Earth-Like Planets Around M Dwarfs”, *Astrobiology* 5, 706–725
- [22] Bean, J. L., J.-M. D’esert, P. Kabath, B. Stalder, S. Seager, E. Miller-Ricci Kempton, Z. K. Berta, D. Homeier, S. Walsh, and A. Seifahrt 2011. “The Optical and Near-infrared Transmission Spectrum of the Super-Earth GJ 1214b: Further Evidence for a Metal-rich Atmosphere”, *ApJ* 743, 92, 12 pp.
- [23] Kreidberg, L., J. L. Bean, J.-M. D’esert, B. Benneke, D. Deming, K. B. Stevenson, S. Seager, Z. Berta-Thompson, A. Seifahrt, and D. Homeier 2014. “Clouds in the atmosphere of the super-Earth exoplanet GJ1214b”, *Nature* 505, 69–72

- [24] Davenport, J. R. A., S. L. Hawley, L. Hebb, J. P. Wisniewski, A. F. Kowalski, E. C. Johnson, M. Malatesta, J. Peraza, M. Keil, S. M. Silverberg, T. C. Jansen, M. S. Scheffler, J. R. Berdis, D. M. Larsen, and E. J. Hilton 2014. “Kepler Flares. II. The Temporal Morphology of White-light Flares on GJ 1243”, *ApJ* 797, 122
- [25] Davenport, J. R. A., D. M. Kipping, D. Sasselov, J. M. Matthews, and C. Cameron 2016. “MOST Observations of Our Nearest Neighbor: Flares on Proxima Centauri”, *ApJ* 829, L31
- [26] Boccaletti, A., C. Thalmann, A.-M. Lagrange, M. Janson, J.-C. Augereau, G. Schneider, J. Milli, C. Grady, J. Debes, M. Langlois, D. Mouillet, T. Henning, C. Dominik, A.-L. Maire, J.-L. Beuzit, J. Carson, K. Dohlen, N. Engler, M. Feldt, T. Fusco, C. Ginski, J. H. Girard, D. Hines, M. Kasper, D. Mawet, F. M’énard, M. R. Meyer, C. Moutou, J. Olofsson, T. Rodigas, J.-F. Sauvage, J. Schlieder, H. M. Schmid, M. Turatto, S. Udry, F. Vakili, A. Vigan, Z. Wahhaj, and J. Wisniewski 2015. “Fast-moving features in the debris disk around AU Microscopii”, *Nature* 526, 230–232
- [27] Hawley, S. L., J. R. A. Davenport, A. F. Kowalski, J. P. Wisniewski, L. Hebb, R. Deitrick, and E. J. Hilton 2014. “Kepler Flares. I. Active and Inactive M Dwarfs”, *ApJ* 797, 121
- [28] King, J. R., A. R. Villarreal, D. R. Soderblom, A. F. Gulliver, and S. J. Adelman 2003. “Stellar Kinematic Groups. II. A Reexamination of the Membership, Activity, and Age of the Ursa Major Group”, *AJ* 125, 1980–2017
- [29] Woitke, P., B. Riaz, G. Duchêne, I. Pascucci, A.-R. Lyo, W. R. F. Dent, N. Phillips, W.-F. Thi, F. M’énard, G. J. Herczeg, E. Bergin, A. Brown, A. Mora, I. Kamp, G. Aresu, S. Brittain, I. de Gregorio-Monsalvo, and G. Sandell 2011. “The unusual protoplanetary disk around the T Tauri star ET Chamaeleontis”, *A&A* 534, A44, 27 pp.
- [30] Hauschildt, P. H., S. Starrfield, S. N. Shore, F. Allard, and E. Baron 1995. “The Physics of Early Nova Spectra”, *ApJ* 447, 829–847
- [31] Barman, T. S., P. H. Hauschildt, C. I. Short, and E. Baron 2000. “A Grid of Non-LTE Model Atmospheres for White Dwarfs in Cataclysmic Variables”, *ApJ* 537, 946–952
- [32] Barman, T. S., P. H. Hauschildt, and F. Allard 2005. “Phase-Dependent Properties of Extrasolar Planet Atmospheres”, *ApJ* 632, 1132–1139
- [33] Short, C. I., and P. H. Hauschildt 2005. “A Non-LTE Line-Blanketed Model of a Solar-Type Star”, *ApJ* 618, 926–938
- [34] Andretta, V., J. G. Doyle, and P. B. Byrne 1997. “The Na I $\lambda\lambda$ 5890,5896 Resonance Doublet as Chromospheric Diagnostics in M dwarfs”, *A&A* 322, 266–279
- [35] Short, C. I., and J. G. Doyle 1998. “Chromospheric modelling of the H α and Na I D lines in five M dwarfs of low to high activity level”, *A&A* 336, 613–625
- [36] Short, C. I., E. A. Campbell, H. Pickup, and P. H. Hauschildt 2012. “Modeling the near-UV Band of GK Stars. II. Non-LTE Models”, *ApJ* 747, 143, 12 pp.
- [37] S. Nikzad, A. D. Jewell, M.E. Hoenk, T.J. Jones, J. Hennessy, Tim Goodsall, Alexander G. Carver, Charles Shapiro, Samuel R. Cheng, Erika T. Hamden, G. Kyne, D.C. Martin, D. Schiminovich, P. Scowen, K. France, S. McCandliss, R.E. Lupu, "High-efficiency UV/optical/NIR detectors for large aperture telescopes and UV explorer missions: development of and field observations with delta-doped arrays," *J. Astron. Telesc. Instrum. Syst.* **3**(3), 036002 (2017), doi: 10.1117/1.JATIS.3.3.036002.
- [38] Hennessy, J., Jewell, A.D., Hoenk, M.E., and Nikzad, S. “Metal-Dielectric Filters for Solar-Blind Silicon Ultraviolet Detectors.” 2015. *Applied Optics* 54: 3507–3512.
- [39] Jewell, A.D., Hennessy, J.; Jones, T., Cheng, S., Carver, A., Ardila, D., Shkolnik, E., Hoenk, M., and Nikzad, S. “Ultraviolet detectors for astrophysics missions: A case study with SPARCS.” 2018. *Proc. SPIE 10709* (in preparation).